Predicting the Elastic Properties and Deformability of Red Blood Cell Membrane Using an Atomistic-Continuum Approach

A.S. Ademiloye, *Member, IAENG,* L.W. Zhang, and K.M. Liew

***Abstract*—This paper employs the gradient theory to study the elastic properties and deformability of red blood cell (RBC) membrane using the first-order Cauchy-Born rule as an atomistic-continuum hyperelastic constitutive model that directly incorporates the microstructure of the spectrin network. The well–known Cauchy–Born rule is extended to account for a three-dimensional (3D) reference configuration. Using the strain energy density function and the deformation gradient tensor, the elastic properties of the RBC membrane were predicted by minimizing the potential energy in the representative cell. This extended formulation was then coupled with the meshfree method for numerical modeling of the finite deformation of the RBC membrane by simulating the optical tweezer experiment using a self–written MATLAB code. The results obtained provide new insight into the elastic properties and deformability of RBC membrane. In addition, the proposed method performs better when compared with those found in literature in terms of prediction accuracy and computation efficiency.**

***Index Terms*—Red blood cells, Cauchy–Born rule, elastic properties, finite deformation, meshfree method, Optical tweezers experiment**

I. Introduction

BLOOD is a bodily fluid in animals that delivers necessary substances such as nutrients and oxygen to the cells and transports metabolic waste products away from the same cells. It is a special fluid, which can be viewed as a suspension of red blood cells (RBCs) or erythrocytes, white blood cells (WBCs) or leukocytes, platelets and blood plasma in a Newtonian fluid. The RBCs alone account for more than 99 % of the particulate matter in blood and about 40–45 % of the blood by volume. The RBCs are biconcave, non-nucleated elastic particles with diameter and thickness of about 8 μm and 10 nm, respectively. Their elastic and mechanical properties are essential for sustaining cell functions. Changes in these properties may eventually lead to the manifestation of various blood related hereditary and non-hereditary diseases.

Recent studies have revealed that the deformability of the red blood cell (RBC) membrane can be assessed experimentally, using atomic force microscopy (AFM), micropipette aspiration technique, optical tweezers, and microfluidic experiments [1]–[4], and numerically, through microscopic, continuum or atomistic–continuum models [5]–[8]. Over the years, the optical tweezers experiment has become a powerful tool for carrying out important biomechanical characterization.

In this study, we carried out numerical simulations to investigate the elastic properties as well as the finite deformation behavior of RBC membrane. In order to map the cell structure in the reference configuration to that in the current deformed configuration directly, the standard Cauchy–Born rule was employed. By using a 3D framework, the in-vivo three-dimensional deformation of RBC membrane can be fully captured. Since this current study involves large deformation, the use of meshfree method is justified due to limitations of mesh-based method [9], [10]. The displacement field comprises of only three nodal displacement degree of freedom because meshfree approximations possess intrinsic non-local properties, leading to real rotation-free approximation hence displacements are the only nodal freedoms present [11].

II. Hyperelastic Constitutive Model

The Cauchy–Born rule [12] establishes a connection between the deformation of the lattice vector of an atomistic system and that of a continuum displacement field, and plays an important role in the development of continuum constitutive models of atomic lattices. In this section, we describe a hyperelastic constitutive model that is derived from the first-order Cauchy–Born rule by using the coarse-grained Helmholtz free energy density to describe the atomic interactions.

Manuscript received December 23, 2015. The work described in this paper was fully supported by grants from the Research Grants Council of the Hong Kong Special Administrative Region, China (Project No. 9042047, CityU 11208914), and National Natural Science Foundation of China (Grant No. 11402142 and Grant No. 51378448).

A. S. Ademiloye is with the Department of Architecture and Civil Engineering, City University of Hong Kong, Tat Chee Avenue, Kowloon, Hong Kong (phone: 852-3442-2749; fax: 852-3442-7612; e-mail: ademiloye.adesola@my.cityu.edu.hk).

L. W. Zhang is with the College of Information Technology, Shanghai Ocean University, Shanghai 201306, PR China (e-mail: zlvwen@hotmail.com).

K. M. Liew is a Chair Professor in the Department of Architecture and Civil Engineering, City University of Hong Kong, Tat Chee Avenue, Kowloon, Hong Kong (phone: 852-3442-6581; fax: 852-3442-7612; e-mail: kmliew@cityu.edu.hk).

ISBN: 978-988-14047-6-3
ISSN: 2078-0958 (Print); ISSN: 2078-0966 (Online)

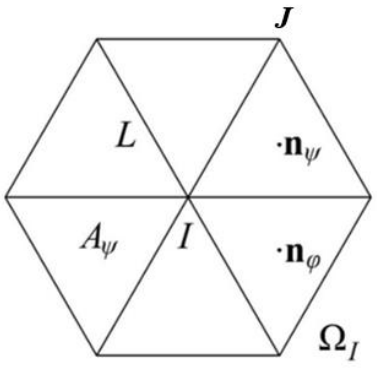

Fig 1. Representative cell of the RBC membrane

Considering a representative cell that is composed of six spectrin links *I–J* (*J* = 1,…, 6) as shown in Fig 1 above, the deformation of each spectrin links can be approximated using the Cauchy-Born rule, as follows,

$$\mathbf{r}_{IJ} \approx \mathbf{F} \cdot \mathbf{R}_{IJ}, \tag{1}$$

where $\mathbf{F} = F_{iJ} e_i \otimes e_J$, $\mathbf{R}_{IJ}$ and $\mathbf{r}_{IJ}$ denotes the first-order deformation gradient tensor, the undeformed and deformed spectrin link length between junction complexes *I* and *J*, respectively.

The strain energy density in this representative cell can be expressed in terms of energy contributions from the in-plane energy, bending energy, surface and volume conservation energy terms [13], as

$$\begin{aligned} W_0 &= W_0(\mathbf{F}) = \frac{V_I}{\Omega_I} \\ &= \frac{1}{\Omega_I}\left[\frac{1}{2}\sum_{J=1}^{6} V_{\mathrm{WLC}}(\mathbf{r}_{IJ}) + \frac{1}{3}\sum_{\psi=1}^{6} C / A_\psi + \sum_{J=1}^{3} V_{\mathrm{bending}}(\bar{k}_b, \theta_{\psi\varphi}) \right. \\ &\qquad \left. + V_{\substack{\mathrm{surface} \\ \mathrm{constraint}}}(\mathbf{r}_{IJ}, k_a) + V_{\substack{\mathrm{volume} \\ \mathrm{constraint}}}(\mathbf{r}_{IJ}, k_v)\right], \end{aligned} \tag{2}$$

where k_a, k_v, and $\bar{k}_b$ are the area, volume constraint and bending coefficients, and Ω_I denotes the area of the representative cell calculated as $\sqrt{3}L^2/2$. For more details, interested readers are referred to the following literature and the references cited therein [7], [14], [15].

III. Elastic Properties of RBC Membrane

In order to determine the elastic properties of RBC membrane, we assume that the elastic deformation of an infinitesimal RBC membrane patch from an initially undeformed planar sheet (Fig 2a) to a deformed planar sheet (Fig 2b) embedded in a 3D space is a simple shear deformation. This shear deformation can be described using the four geometrical parameters $\lambda_1, \lambda_2, \lambda_3$, and θ, whose deformation map and gradient can be expressed as follows,

$$\begin{aligned} x_1 &= \lambda_1 X_1 \\ x_2 &= \lambda_2 X_2 + \lambda_1 X_1 \theta \\ x_3 &= \lambda_3 X_3 \end{aligned}, \tag{3}$$

$$\mathbf{F} = \frac{\partial \mathbf{x}}{\partial \mathbf{X}} = \begin{bmatrix} \lambda_1 & 0 & 0 \\ \lambda_1\theta & \lambda_2 & 0 \\ 0 & 0 & \lambda_3 \end{bmatrix}. \tag{4}$$

The optimal values of the geometrical parameters in (3) and (4) can be obtained by minimizing the strain energy density using the Newton's method.

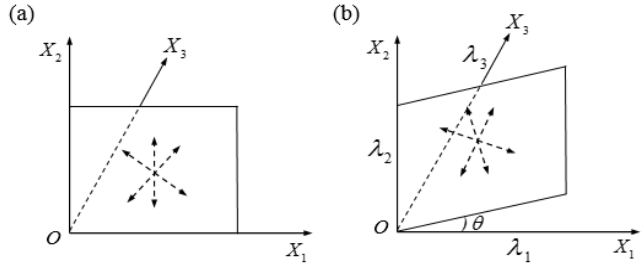

Fig 2. Simple shear deformation of an infinitesimal patch on the RBC membrane surface (a) reference configuration, (b) current configuration

Once the minimization step is completed, the first-order Piola–Kirchhoff stress tensor **P** and the tangent modulus, $\mathbf{M}^{FF}$ are the first- and second-order derivative of the strain energy density with respected to **F**, respectively can be calculated using,

$$\begin{aligned} \mathbf{P} &= \frac{\partial W_0}{\partial \mathbf{F}} = \left[\frac{\partial \mathbf{r}_{IJ}}{\partial \mathbf{F}}\right] \bullet \left[\frac{\partial W_0}{\partial \mathbf{r}_{IJ}}\right], \\ \mathbf{M}^{FF} &= \frac{\partial^2 W_0}{\partial \mathbf{F}^2} = \left[\frac{\partial \mathbf{r}_{IJ}}{\partial \mathbf{F}}\right] \bullet \left[\frac{\partial^2 W_0}{\partial \mathbf{r}_{IJ}^{\,2}}\right] \bullet \left[\frac{\partial \mathbf{r}_{IJ}}{\partial \mathbf{F}}\right]^{\mathrm{T}}. \end{aligned} \tag{5}$$

The Young's modulus *E*, Poisson's ratio ν, shear modulus μ_h, area compression modulus *K*, and bending modulus *B* of the RBC membrane can be obtained using the expressions below:

$$\begin{aligned} E &= \mathbf{M}^{FF}_{1111} - (\mathbf{M}^{2}_{1122} / \mathbf{M}^{FF}_{2222}), \\ \nu &= \mathbf{M}^{FF}_{1122} / \mathbf{M}^{FF}_{2222}, \\ \mu_h &= 0.5 \times (\mathbf{M}^{FF}_{2222} - \mathbf{M}^{FF}_{1122}), \\ K &= 0.5 \times (\mathbf{M}^{FF}_{2222} + \mathbf{M}^{FF}_{1122}), \\ B &= 0.5\eta^2 \times (\mathbf{M}^{FF}_{2222} - \mathbf{M}^{FF}_{1122}), \end{aligned} \tag{6}$$

where η is an elastic length scale, taken as $0.28\ \mu\mathrm{m}$ [16]. The microstructure parameter set used in the study are as follows: initial equilibrium spectrin length *L* = 87 nm, persistence length *p* = 8.5 nm, maximum spectrin extension length $L_{\max}$ = 238 nm, number of triangular face on RBC membrane surface N_f = 41192, bending coefficient $\bar{k}_b$ = 2.77 × 10^{-19} J, and temperature *T* = 300 K.

Using the models given in (6) and the algorithm described above, we computed the elastic properties of the RBC membrane as shown in Table I below.

ISBN: 978-988-14047-6-3
ISSN: 2078-0958 (Print); ISSN: 2078-0966 (Online)

TABLE I
VALUES OF ELASTIC PROPERTIES OF RBC MEMBRANE IN COMPARISON WITH THOSE IN LITERATURE FOR DIFFERENT VALUE OF k_a AND k_v.

Elastic Properties (units)	$k_a = k_v = \xi$		
	$\xi = 0$	ξ = [100 (150) 300]	References
E (μN/m)	22.13	21.42 (19.31) 17.31	22.11 ($\xi = 0$) [17], 13.80 – 18.40 [18], 19.0 – 33.0 [1].
ν	0.33	0.46 (0.45) 0.44	0.33 ($\xi = 0$) [17], ~ 0.50 [19], 0.49 [20].
μ_h (μN/m)	7.98	7.49 (6.70) 6.00	8.30 ($\xi = 0$) [17], 5.50 – 8.70 [21].
K (μN/m)	15.96	20.14 (17.65) 15.55	16.60 ($\xi = 0$) [17], 12.10 – 18.7 [21].
B ($\times 10^{-19}$ J)	6.26	5.87 (5.25) 4.71	2.0 – 7.0 [22], ~ 9.0 [23].

IV. ATOMISTIC-CONTINUUM MESHFREE METHOD

Based on the constitutive relations in section II, a computational scheme can be established to perform the numerical simulation of RBC membrane deformation. The meshfree method is a computational technique that has some excellent advantages over the classical finite element method. In particular, meshfree approximations have non-local properties, and satisfy the higher order continuity requirement [10]. The intrinsic non-local property of meshfree interpolation leads to real rotation-free approximation, and displacements can thus be used as the only nodal freedoms [11]. Improved moving least squares (IMLS) approximation [24] is used to construct the meshfree interpolation and can be combined with the Ritz minimization procedure to form the IMLS-Ritz meshfree method.

In the computation, we considered the RBC as a body that initially occupies a region Ω^0 and deforms to a new configuration Ω^t. The deformation of a material particle $\mathbf{X} \in \Omega^0$ at a time t is described by $\mathbf{x}(\mathbf{X}, t)$ through the mapping functions ϕ as

$$\mathbf{x}(\mathbf{X}, t) = \mathbf{u}(\mathbf{X}, t) + \mathbf{X} \tag{7}$$

where $\mathbf{u}$ is the displacement of this material particle. The first-order deformation gradients $\mathbf{F}$ can therefore be defined as

$$F_{ij} = \frac{\partial x_i}{\partial X_j} = \frac{\partial u_i}{\partial X_j} + \delta_{ij}, \quad i, j = 1, 2, 3. \tag{8}$$

or

$$\mathbf{F} = \frac{\partial \mathbf{x}}{\partial \mathbf{X}} = \frac{\partial \mathbf{u}}{\partial \mathbf{X}} + \mathbf{I}, \tag{9}$$

where δ_{ij} is the kronecker delta property.

The displacements relative to the undeformed cell configuration are approximated as

$$\mathbf{u} = \sum_{I=1}^{NP} \tilde{\Phi}_I(x) \cdot \dot{u}_I(t) = \tilde{\mathbf{\Phi}}(x)\dot{\mathbf{u}} \tag{10}$$

where $\dot{\mathbf{u}}$ denotes the nodal parameter, $\tilde{\Phi}_I$ the meshfree interpolation (or shape) function derived using the IMLS approximation at the *I*th node and *NP* is the total number of nodes covered by the compact support domain. By treating the RBC membrane as a 2D surface embedded in a 3D space, all nodes have three degree of freedom. The 3D IMLS shape function with linear basis and circular support domain were employed.

The first-order deformation gradients **F** corresponding to the displacement step above are approximated by using (9) and (10) above, as

$$\mathbf{F} = \sum_{I=1}^{NP} \nabla_X (\tilde{\Phi}_I . \dot{u}_I) = \sum_{I=1}^{NP} \begin{bmatrix} \tilde{\Phi}_{I,1} \\ \tilde{\Phi}_{I,2} \\ \tilde{\Phi}_{I,3} \end{bmatrix} . \dot{u}_I + \mathbf{I}, \tag{11}$$

where $\tilde{\Phi}_{I,K}$ (K = 1,2,3) is the first-order derivative of the meshfree shape function with respect to the reference configuration.

The total energy of the system can be calculated as:

$$\prod = \int_{\Omega_0} W(\mathbf{F}) d\Omega - \int_{\Omega_0} \mathbf{u} \cdot \boldsymbol{b}_0 d\Omega - \int_{\partial\Omega} \mathbf{u} \cdot \boldsymbol{t}_0^P dS, \tag{12}$$

where $W(\mathbf{F}) = hW_0(\mathbf{F})$ is the strain energy density function adopted in order to incorporate the effect of membrane thickness h, $\boldsymbol{t}_0^P$ represent the first-order stress tractions on the surface of the domain. Contribution from body force term was neglected. The Ritz parameters are determined (or adjusted) such that $\delta\Pi = 0$. For simulations in this section, contributions from area and volume conservation energy were ignored for the sake of simplicity.

Upon discretizing (8) above using the well-known meshfree and finite elasticity framework, the resulting incremental system equations can be written as

$$\mathbf{K}_{n+1} \Delta\dot{\mathbf{u}}_{n+1} = \mathbf{f}_{n+1}, \tag{13}$$

where $\Delta\dot{\mathbf{u}}_{n+1}$ contains the nodal parameters of all meshfree nodes. $\mathbf{K}_{n+1}$ and $\mathbf{f}_{n+1}$ represents the global stiffness matrix and non-equilibrium force vector, and they are given by

$$\begin{aligned} \mathbf{K}_{n+1} &= \int_\Omega [\mathbf{B}^T \cdot \mathbf{M}^{FF} \cdot \mathbf{B}] d\Omega \\ &= \int_\Omega [(\mathbf{L} \cdot \tilde{\mathbf{\Phi}})^T \cdot \mathbf{M}^{FF} \cdot (\mathbf{L} \cdot \tilde{\mathbf{\Phi}})] d\Omega \end{aligned}, \tag{14}$$

$$\begin{aligned} \mathbf{f}_{n+1} &= \mathbf{f}_{n+1}^{ext} - \mathbf{f}_{n+1}^{int} = \int_{\partial\Omega} \tilde{\mathbf{\Phi}}^T \boldsymbol{t}_0^P dS - \int_\Omega \mathbf{B}^T \cdot \mathbf{P}_n d\Omega \\ &= \int_{\partial\Omega} \tilde{\mathbf{\Phi}}^T \boldsymbol{t}_0^P dS - \int_\Omega (\mathbf{L} \cdot \tilde{\mathbf{\Phi}})^T \cdot \mathbf{P}_n d\Omega \end{aligned}, \tag{15}$$

where $\mathbf{P}_n$ denotes assembled stress vector at the time t when the stress components are known and $\mathbf{L}$ is an assembled differential operator matrix with respect to the undeformed cell configuration,

ISBN: 978-988-14047-6-3
ISSN: 2078-0958 (Print); ISSN: 2078-0966 (Online)

$$\mathbf{L}=\begin{bmatrix} \partial/\partial X_1 & 0 & 0 \\ \partial/\partial X_2 & 0 & 0 \\ \partial/\partial X_3 & 0 & 0 \\ 0 & \partial/\partial X_1 & 0 \\ 0 & \partial/\partial X_2 & 0 \\ 0 & \partial/\partial X_3 & 0 \\ 0 & 0 & \partial/\partial X_1 \\ 0 & 0 & \partial/\partial X_2 \\ 0 & 0 & \partial/\partial X_3 \end{bmatrix}. \quad (16)$$

The stiffness matrix in (14) and the internal force vector in (15) are integrated using the Gauss quadrature integration techniques while the external force vector in (15) was computed using the direct nodal force application technique.

In the present study, a simple technique is used to ensure that the solution converges to the minimum point. This was achieved by replacing $\mathbf{K}_{n+1}$ with $\mathbf{K}_{n+1}+\alpha\mathbf{I}$, where α is a positive number that is slightly larger than the magnitude of the most negative eigenvalue of $\mathbf{K}_{n+1}$, and $\mathbf{I}$ is an identity matrix. After a few cycles of replacements, $\mathbf{K}_{n+1}$ becomes positive definite and the standard Newton method continues.

V. Finite Deformation of the RBC Membrane

Using the present meshfree method, we have studied the finite deformation behavior of the RBC membrane. This was achieved by simulating the optical tweezers techniques, in which two silica beads trapped by laser beams are attached to left and right ends of the cell. The trapped cell was stretched by fixing one of the beads and pulling the other in an axial, as illustrated in Fig 3.

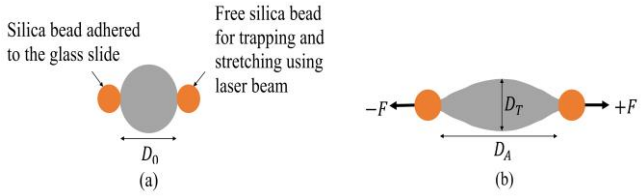

Fig 3. Optical tweezer experiment setup and computational configuration adopted in this study.

The axial (D_A) and transverse (D_T) diameters of the stretched cell, corresponding to the applied stretching force were recorded. The total stretching force, $+F$ within the range $0-180$ pN was applied to $N_+ = \ell N_v$ vertices of the problem domain with the largest x-coordinates in the positive x-direction, then a corresponding equal but opposite force, $-F$ was exerted on $N_- = \ell N_v$ vertices with the smallest x-coordinates in the negative x-directions. The value of ℓ was taken to be 0.05 which represents the number of nodes in contact with the attached silica beads. The simulations for each given stretching force within the force range were performed lambda (λ) times, where λ correspond to the maximum number of loading steps adopted. The external force vector $\mathbf{f}_{n+1}^{ext}$ is assembled from the total stretching forces, $+F$ and $-F$.

Within each loading step, iteration was performed until the solution converges, after which the next loading step starts. At the end of the final loading steps, the undeformed RBC geometry was updated to obtain the final deformed geometry. The deformed axial diameter, D_A was then computed as $|x_{\max}-x_{\min}|$, where $x_{\max}$ is the maximum x coordinate among the N_+ vertices, and $x_{\min}$ is the minimum among N_- vertices. Also, the deformed transverse diameter, D_T was obtained using the expression $2\times\max_{j=1\ldots N_v}\sqrt{(y_j)^2+(z_j)^2}$, where y_j and z_j are coordinate value of each vertices in y and z directions, and N_v represents the total number of meshfree nodes discretized on the problem domain as shown in Fig 4 below.

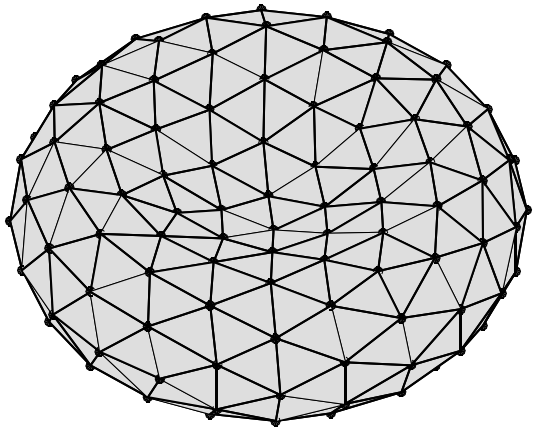

Fig 4. Full geometry of RBC membrane (problem domain) showing meshfree node distributions and triangular meshes as visualization aid.

This simulation was performed using 162 meshfree nodes, quadrilateral background cell for numerical integration, cubic spline weight function, meshfree scaling parameter $d_{\max}=1.462$, 17 loading step and RBC membrane parameter set: RBC diameter $D_0=7.82$ µm, $L=87$ nm, $p=8.5$ nm, $L_{\max}=238$ nm, temperature T = 300 K, and assumed membrane thickness t = 12 nm.

Fig 5 below shows the comparison between our current meshfree simulation, spectrin level modeling, quasi-continuum meshfree simulation as well as the optical tweezer experiment. From the plotted figure, the performance of the newly implemented approach is obviously better as the obtained values for stretched axial and transverse diameters for each stretching force are very close to those observed in the experiment.

ISBN: 978-988-14047-6-3
ISSN: 2078-0958 (Print); ISSN: 2078-0966 (Online)

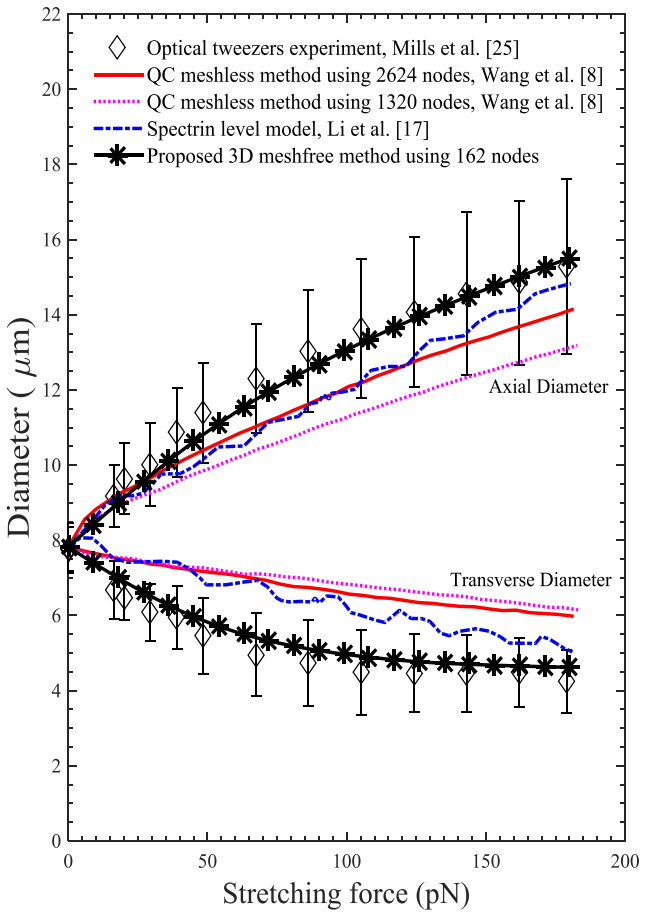

Fig 5. Axial and transverse diameter of RBC membrane as a function of stretching force in comparison with optical tweezer experiment [25], quasi-continuum meshfree simulations [8] and spectrin level modeling [17].

VI. Conclusion

The elastic properties and deformability of the RBC membrane were studied in this paper using a gradient theory based on the standard Cauchy–Born rule. The elastic moduli of the RBC membrane were obtained using the strain energy density function and deformation gradient tensor by minimizing the energy in the representative cell. An atomistic-continuum meshfree method was also implemented to study the three-dimensional finite deformation of the RBC membrane by simulating the optical tweezers experiment. Results obtained from this study were presented in comparison with those in literature and we conclude that the present approach gives reasonable predictions for both the elastic properties and RBC membrane deformability. Furthermore, since the proposed meshfree analysis with fewer nodes on the problem domain give better predictions than previous numerical studies, we conclude that the current approach is computationally efficient.

References

[1] I. Dulińska, M. Targosz, W. Strojny, M. Lekka, P. Czuba, W. Balwierz, et al., Stiffness of normal and pathological erythrocytes studied by means of atomic force microscopy, *J. Biochem. Biophys. Methods*. 66 (2006) 1–11. doi:10.1016/j.jbbm.2005.11.003.

[2] E.A. Evans, New membrane concept applied to the analysis of fluid shear- and micropipette-deformed red blood cells., *Biophys. J.* 13 (1973) 941–954. doi:10.1016/S0006-3495(73)86036-9.

[3] S. Henon, G. Lenormand, A. Richert, F. Gallet, A new determination of the shear modulus of the human erythrocyte membrane using optical tweezers, *Biophys. J.* 76 (1999) 1145–1151.

[4] D.J. Quinn, I. Pivkin, S.Y. Wong, K.H. Chiam, M. Dao, G.E. Karniadakis, et al., Combined simulation and experimental study of large deformation of red blood cells in microfluidic systems, *Ann. Biomed. Eng.* 39 (2011) 1041–50. doi:10.1007/s10439-010-0232-y.

[5] T. Klöppel, W.A. Wall, A novel two-layer, coupled finite element approach for modeling the nonlinear elastic and viscoelastic behavior of human erythrocytes, *Biomech. Model. Mechanobiol.* 10 (2011) 445–459. doi:10.1007/s10237-010-0246-2.

[6] I. Pivkin, G. Karniadakis, Accurate Coarse-Grained Modeling of Red Blood Cells, *Phys. Rev. Lett.* 101 (2008) 118105.

[7] A.S. Ademiloye, L.W. Zhang, K.M. Liew, Numerical computation of the elastic and mechanical properties of red blood cell membrane using the higher-order Cauchy–Born rule, *Appl. Math. Comput.* 268 (2015) 334–353. doi:10.1016/j.amc.2015.06.071.

[8] X. Wang, X. Guo, Z. Su, A quasi-continuum model for human erythrocyte membrane based on the higher order Cauchy–Born rule, *Comput. Methods Appl. Mech. Eng.* 268 (2014) 284–298.

[9] S. Li, W.K. Liu, Meshfree and particle methods and their applications, *Appl. Mech. Rev.* 55 (2002) 1. doi:10.1115/1.1431547.

[10] V.P. Nguyen, T. Rabczuk, S. Bordas, M. Duflot, Meshless methods: a review and computer implementation aspects, *Math. Comput. Simulat.* 79 (2008) 763-813. doi:10.1016/j.matcom.2008.01.003.

[11] Z. Tang, S. Shen, S.N. Atluri, Analysis of materials with strain-gradient effects: A meshless local Petrov-Galerkin (MLPG) approach, with nodal displacements only, *Comput. Model. Eng. Sci.* 4 (2003) 177–196.

[12] E. Tadmor, G. Smith, N. Bernstein, E. Kaxiras, Mixed finite element and atomistic formulation for complex crystals, *Phys. Rev. B.* 59 (1999) 235–245. doi:10.1103/PhysRevB.59.235.

[13] D.E. Discher, S.K. Boey, D.H. Boal, Simulations of the erythrocyte cytoskeleton at large deformation. II. Micropipette aspiration, *Biophys. J.* 75 (1998) 1584–97.

[14] Y. Sun, K.M. Liew, Mesh-free simulation of single-walled carbon nanotubes using higher order Cauchy-Born rule, *Comput. Mater. Sci.* 42 (2008) 444–452. doi:10.1016/j.commatsci.2007.08.008.

[15] P. Xiang, K.M. Liew, A computational framework for transverse compression of microtubules based on a higher-order Cauchy-Born rule, *Comput. Methods Appl. Mech. Eng.* 254 (2013) 14–30.

[16] R. Mukhopadhyay, G.L.H. W, M. Wortis, B. Columbia, H.W. Gerald Lim, Echinocyte Shapes: Bending, Stretching, and Shear Determine Spicule Shape and Spacing, *Biophys. J.* 82 (2002) 1756–1772.

[17] J. Li, M. Dao, C.T. Lim, S. Suresh, Spectrin-level modeling of the cytoskeleton and optical tweezers stretching of the erythrocyte., *Biophys. J.* 88 (2005) 3707–3719. doi:10.1529/biophysj.104.047332.

[18] A.A. Bukharaev, A.A. Mozhanova, N.I. Nurgazizov, D. V Ovchinnikov, Measuring local elastic properties of cell surfaces and soft materials in liquid by atomic force microscopy, *Phys. Low-Dimensional Struct.* 3 (2003) 31–37.

[19] Y.C. Fung, *Biomechanics: Mechanical Properties of Living Tissues*, second ed., Springer Science+Business Media, LLC, New York, 1993. doi:10.1097/00024382-199802000-00018.

[20] M. Radmacher, Measuring the elastic properties of biological samples with the AFM, *Eng. Med. Biol. Mag. IEEE*. 16 (1997) 47–57.

[21] H. Byun, T.R. Hillman, J.M. Higgins, M. Diez-Silva, Z. Peng, M. Dao, et al., Optical measurement of biomechanical properties of individual erythrocytes from a sickle cell patient, *Acta Biomater.* 8 (2012) 4130–8. doi:10.1016/j.actbio.2012.07.011.

[22] H. Strey, M. Peterson, E. Sackmann, Measurement of erythrocyte membrane elasticity by flicker eigenmode decomposition., *Biophys. J.* 69 (1995) 478–488. doi:10.1016/S0006-3495(95)79921-0.

[23] J. Evans, W. Gratzer, N. Mohandas, K. Parker, J. Sleep, Fluctuations of the red blood cell membrane: relation to mechanical properties and lack of ATP dependence, *Biophys. J.* 94 (2008) 4134–44.

[24] Z. Zhang, K.M. Liew, Y. Cheng, Y.Y. Lee, Analyzing 2D fracture problems with the improved element-free Galerkin method, *Eng. Anal. Bound. Elem.* 32 (2008) 241–250.

[25] J.P. Mills, L. Qie, M. Dao, C.T. Lim, S. Suresh, Nonlinear elastic and viscoelastic deformation of the human red blood cell with optical tweezers, *Mech. Chem. Biosyst.* 1 (2004) 169–80.

ISBN: 978-988-14047-6-3
ISSN: 2078-0958 (Print); ISSN: 2078-0966 (Online)